

The Cores of the Fe K Lines in Seyfert I Galaxies Observed by the Chandra High Energy Grating

Tahir Yaqoob^{a b} & Urmila Padmanabhan^a

^a*Department of Physics and Astronomy, Johns Hopkins University, Baltimore, MD 21218.*

^b*Laboratory for High Energy Astrophysics, NASA/Goddard Space Flight Center, Greenbelt, MD 20771.*

Abstract

We report on the results of eighteen observations of the core, or peak, of the Fe K α emission line at ~ 6.4 keV in fifteen Seyfert I galaxies using the *Chandra* High Energy Grating (HEG). These data afford the highest precision measurements of the peak energy of the Fe K α line, and the highest spectral resolution measurements of the width of the core of the line to date. We were able to measure the peak energy in seventeen data sets, and, excluding a very deep observation of NGC 3783, we obtained a weighted mean of 6.404 ± 0.005 keV. In all fifteen sources the two-parameter, 99% confidence errors on the line peak energy do not exclude fluorescent K α line emission from Fe I, although two sources (Mkn 509 and 3C 120) stand out as very likely being dominated by K α emission from Fe XVII or so. We were able to measure the line core width in fourteen data sets and obtained a weighted mean of 2380 ± 760 km s $^{-1}$ FWHM (excluding the NGC 3783 deep exposure), a little larger than the instrument resolution (~ 1860 km s $^{-1}$ FWHM). However, there is evidence of underlying broad line emission in at least four sources. In fact, the width of the peak varies widely from source to source and it may in general have a contribution from the outer parts of an accretion disk *and* more distant matter. For the disk contribution to also peak at 6.4 keV requires greater line emissivity at hundreds of gravitational radii than has been deduced from previous studies of the Fe K α line.

Keywords: accretion disks – galaxies: active – line: profile – X-rays: galaxies

Accepted for Publication in the Astrophysical Journal 21 November 2003

1. INTRODUCTION

At least part of the Fe K α fluorescent emission line in type I active galactic nuclei (AGNs) is believed to originate in a relativistic accretion disk around a black hole (e.g. see reviews by Fabian *et al.* 2000; Reynolds & Nowak 2003). The dominant peak energy of the Fe K α line at ~ 6.4 keV appears to be ubiquitous and this core of the line carries a substantial fraction of the total line flux (e.g. Nandra *et al.* 1997a; Sulentic *et al.* 1998; Lubiński & Zdziarski 2001; Weaver, Gelbord, & Yaqoob 2001; Yaqoob *et al.* 2002; Perola *et al.* 2002; Reeves 2002). Often, the broad part of the Fe K α line is absent, leaving only the narrow core. It has been traditional to associate such narrow Fe K α lines with an origin in distant matter, at least several thousand gravitational radii from the putative black hole (e.g. the optical broad-line region (BLR), the putative obscuring torus, or the optical narrow-line region (NLR)). However, Petrucci *et al.* (2002) recently reported a *variable*, narrow Fe K α line in Mkn 841, supporting an accretion-disk origin. Moreover, rapidly vari-

able, narrow Fe K line emission has been observed in the Seyfert I galaxy NGC 7314 (Yaqoob *et al.* 2003a). Thus, even narrow Fe K α lines may have a significant contribution from the accretion disk (Lee *et al.* 2002; Yaqoob *et al.* 2003a). While such lines may be interpreted in terms of a truncated disk (e.g. Done, Madejski, & Życki 2000), they could be due to low-inclination angle disks with a flat radial line emissivity (i.e. intensity per unit area falling off with radius more slowly than r^{-2}).

In this paper we address two very specific questions, using the *Chandra* high energy grating transmission spectrometer (*HETGS*; see Markert *et al.* 1995), which affords the best spectral resolution currently available at 6.4 keV (~ 39 eV, or ~ 1860 km s $^{-1}$ FWHM). Namely, for a sample of type I AGNs, what are the energies of the peaks of the Fe K line emission and are these line cores resolved by *Chandra*? This information can give important clues about the ionization state of Fe responsible for the line emission, and its origin. With *Chandra* we can measure the peak energies with better precision than *ASCA*, at least by a

factor of four.

We note that, due to the small throughput of the *HETGS* (especially above ~ 7 keV), it is very difficult for the grating data to constrain the parameters of any underlying broad Fe K α line emission. However, in a different study we shall systematically compare the total Fe K α line emission observed with *Chandra* and *ASCA* data and show that, aside from variability in some sources, there is good agreement between the two sets of data. We emphasize that even though the *Chandra* data for most type I AGN show narrow Fe K α line peaks, this by no means indicates that there is no broad Fe K α line emission.

2. OBSERVATIONS AND DATA

Our study is based on eighteen observations of fifteen type I AGN (see Table 1) with $z < 0.05$ observed with *HETGS*, that were in the *Chandra* public archives as of 2003, July 1, and had a total, first-order, HEG count rate higher than 0.05 ct/s. Blazars, BL Lac objects, and AGN that are intermediate between type I and type II were excluded from the study. Details of all the observations can be found from the *Chandra* public archive¹. Three sources were observed more than once: NGC 3516, NGC 5548, and NGC 3783. For NGC 3516, observation IDs 2080 and 2431 were combined since they occurred on consecutive days, whilst observation ID 2482 was treated separately (see also Turner *et al.* 2002). The two observations of NGC 5548 were treated separately. For NGC 3783, six observations were at first treated separately but we found that the Fe K line parameters were consistent with no variability, so here we report the results from the ~ 850 ks spectrum combined from five snapshots taken during a monitoring campaign but treated this separately from an observation made a year earlier. Detailed results from the monitoring campaign will be presented elsewhere (Yaqoob *et al.*, in preparation; see also Kaspi *et al.* 2002, and Netzer *et al.* 2003).

HETGS consists of two grating assemblies, a High-Energy Grating (HEG) and a Medium-Energy Grating (MEG), and it is the HEG that achieves the highest spectral resolution. The MEG has only half of the spectral resolution of the HEG and less effective area in the Fe-K band, so our study will focus on the HEG data.

The *Chandra* data were reduced and HEG spectra made, exactly as described in Yaqoob *et al.* (2003b). We used only the first orders of the grating data (combining the positive and negative arms). The mean HEG count rates ranged from 0.087 ct/s for the weakest source (NGC 3227) to 1.16 ± 0.006 for the brightest source (IC 4329a). The exposure time ranged from ~ 40 ks to ~ 850 ks, but was $\sim 60 - 100$ ks for most of the sources. Background was not subtracted since it is negligible over the energy range of interest (e.g. see Yaqoob *et al.* 2003a). Note that the systematic uncertainty in the HEG wavelength scale is $\sim 433 \text{ km s}^{-1}$ ($\sim 11 \text{ eV}$) at 6.4 keV ².

3. SPECTRAL FITTING RESULTS

We used XSPEC v11.2 (Arnaud 1996) for spectral fitting. Since we are interested in utilizing the highest possible spectral resolution available, we used spectra binned at 0.0025 \AA , and this amply oversamples the HEG resolution (0.012 \AA FWHM). The *C*-statistic was used for minimization. All model parameters will be referred to the source frame. Our method is simply to fit a simple power-law plus Gaussian emission-line model over the 2–7 keV band for each spectrum. NGC 3516 required photoelectric absorption to fit the continuum. Also, for NGC 7314 the analysis was more complex, involving emission from multiple ionization states of Fe, and has already been described in detail in Yaqoob *et al.* (2003a). The results presented here for NGC 7314 are for the 6.4 keV line component only (which is unresolved) and have been taken from Yaqoob *et al.* (2003a), changing only the confidence levels of the quoted statistical errors so that they are consistent with the rest of the sample. For Akn 564 an Fe K emission line was not detected: *C* decreased by 0.9 ($< 68\%$ confidence for the addition of one free parameter) when a narrow (FWHM much less than the instrument resolution) emission line at 6.4 keV was added to a power-law only. Thus, we obtained upper limits on the equivalent width (EW). A significant Fe K emission line has been detected in Akn 564 with *ASCA* (Turner *et al.* 2001). The reason for the non-detection by the HEG is likely to be due to the very steep continuum and the small effective area of the HEG. The line was only weakly detected during recent *XMM-Newton* observations (Vignali *et al.* 2003),

¹<http://cda.harvard.edu:9011/chaser/>

²<http://space.mit.edu/CXC/calib/hetgcal.html>

but the signal-to-noise of those data was still much less than that of the *ASCA* data. In the case of NGC 3227 and Mkn 766 the detection of an Fe K line was marginal: C decreased by 4.5 and 7.0 respectively, when a narrow Gaussian was added to a power-law model only. In this case we were able to obtain constraints on the line energy and EW, so the Gaussian model had two free parameters. Thus, the lines were detected with $< 90\%$ and $< 95\%$ confidence in NGC 3227 and Mkn 766 respectively. Note that a strong Fe K line has been detected in NGC 3227 by *XMM-Newton* (Gondoin *et al.* 2003), and complex Fe K emission has been observed in Mkn 766 by *XMM-Newton* (Pounds *et al.* 2003). For the remaining spectra the Gaussian component had three free parameters (line center energy, width, and intensity). Thus, except for the three cases mentioned above, the model had five free parameters in total, including the continuum slope and normalization.

We used the ‘goodness’ command in XSPEC to assess the goodness of the fits: this command performs Monte Carlo simulations of spectra using the best-fitting model and gives the percentage of the simulated spectra that had a fit statistic less than that obtained from the fit to the real data. A value of 50% is expected if the best-fitting model is a good representation of the data. Values much less than 50% indicate that the data are over-parameterized by the model since random statistical fluctuations in the majority of the simulated spectra are not able to produce a fit statistic as low as that obtained from the real data. In the opposite limit, when 100% of the simulated spectra have a fit statistic less than that obtained from the real data, the fit is clearly poor.

Good fits were obtained for all spectra except for NGC 3783(2), the long ~ 850 ks observation, in which the continuum is complicated by a warm absorber that affects the spectrum even above 2 keV (e.g. see Kaspi *et al.* 2002, and Netzer *et al.* 2003). However, this has little impact on the deduced parameters of the Fe K α line which are in fact consistent with those obtained by Kaspi *et al.* (2002) and Netzer *et al.* (2003), who used a more complex continuum. The line parameters, including the intensity, are also consistent with those measured from a non-simultaneous *XMM-Newton* observation (Reeves *et al.* 2004), for which a warm absorber was also included in the continuum modeling.

Excluding Akn 564, NGC 3227, and Mkn 766,

the Fe K α line core was detected at a confidence level $> 3\sigma$ (corresponding to a decrease in C greater than 14.16 when a Gaussian with three free parameters was added to the continuum). Five of these fifteen spectra gave ‘goodness’ values less than 50%. Two of these were close to 50% (NGC 4051: 49%, F 9: 47%) so the data are likely not over-parameterized. Also, C decreased by 33.2 and 26.6 for NGC 4051 and F 9 respectively, when a three-parameter Gaussian model was added to the continuum model. Thus the line-emission was detected at a confidence level $> 5\sigma$ and $> 4\sigma$ in NGC 4051 and F 9 respectively. In the other three cases, the goodness values were 32% (Mkn 509), 10% (NGC 3516(2)), and 7%(NGC 5548(1)). In the case of Mkn 509, when the data were modeled without an emission line, the ‘goodness’ value was 40%, still less than 50%, indicating that the signal-to-noise over the entire energy band is poor. The decrease in C when a Gaussian is added to the continuum is 16.8, which still corresponds to a detection at a confidence level $> 3\sigma$, for the addition of three free parameters. For NGC 3516(1), the ‘goodness’ value increases from 10% to 69% when the emission line is removed and the data fitted with a continuum only. The addition of a three-parameter Gaussian to the continuum decreases C by 111.4, confirming what is evident from the spectrum in Fig. 1, that the line emission is highly significant and required by the data. In the case of NGC 5548(1), removing the emission line and fitting a continuum only, increases the ‘goodness’ value from 7% to 18%, still below 50%. However, the addition of a three-parameter Gaussian to the continuum decreases C by 35.0, indicating that the Fe K α line is detected at a confidence level $> 5\sigma$. The low values of the ‘goodness’ parameter are due to poor signal-to-noise over the whole energy band since a simple two-parameter continuum gives a ‘goodness’ value much less than 50%.

Although the Fe K α line consists of two components ($K\alpha_1$ and $K\alpha_2$, separated by 13 eV), we modeled it as a single Gaussian, since it was shown in Yaqoob *et al.* (2001), that with the spectral resolution of the HEG, there is a negligible impact on the measured line width. Some broadening may also result from the presence of line emission from more than one ionization state of Fe. However, we do not interpret the measured FWHM velocities literally. Also, the use of a sin-

gle Gaussian (without any attempt to model the underlying broad Fe K α emission) also has a negligible impact on the measured center energy of the core, the line intensity and EW (see Yaqoob *et al.* 2001). Again, we only interpret the line intensity and EW qualitatively. Furthermore, one of the reasons for measuring the width of the line core is to obtain clues about any underlying broad Fe K α line component.

The best-fitting emission-line parameters for each spectrum are shown in Table 1 (as well as extrapolated 2–10 keV fluxes and luminosities). Note that since the models were fitted by first folding through the instrument response before comparing with the data, the derived line parameters *do not* need to be corrected for instrumental response. In order that the results can be used for future statistical analyses the statistical errors shown correspond to 68% confidence ($\Delta C = 3.506, 2.279$, or 0.989 , depending on whether there were 3, 2 or 1 free parameter(s) free in the Gaussian component). However, as a more conservative measure, the 90% confidence range for each line parameter is also given in Table 1. Fig. 1 shows each of the eighteen spectra in the Fe K region, corrected for instrumental efficiency and cosmological redshift. The spectra are binned at 0.01\AA , similar to the HEG spectral resolution of 0.012\AA , so broad features are not readily discernable in this representation.

4. PROPERTIES OF THE CORE OF THE FE K LINE EMISSION

Fig. 2 shows joint, 99% confidence contours of the line intensity versus line center energy for thirteen of the eighteen spectra, and Fig. 3 shows the 99% confidence contours of the line EW versus FWHM width for the same spectra. Excluded were Mkn 766, NGC 3227, and Akn 564, (since the constraints on the line parameters are poor), the short, first observation of NGC 3783 (since the later observation had ~ 20 times the exposure time), and NGC 7314 (that has complex Fe K emission from multiple ionization states: see Yaqoob *et al.* 2003a).

Fig. 2 and Fig. 3 show the results for the eleven sources, split into two groups. Group 1 (Fig. 2 (a) and Fig. 3 (a)) is comprised of NGC 3516, Mkn 509, NGC 5548, 3C 120, NGC 3783, and MCG -6-30-15. Group 2 (Fig. 2 (b) and Fig. 3 (b)) is comprised of NGC 4593, Mkn 279,

NGC 4051, IC 4329a, and F 9. Roughly speaking, group 1 AGN have more prominent narrow Fe K line cores than group 2, as evidenced by the larger contours for group 2. In fact, for NGC 4593 and NGC 4051 the 99% contours could not be well constrained because when the Gaussian is very broad, there is a lot of interaction between the line width and the continuum slope, particularly if there is a reflection continuum, which we have not modeled here. Therefore we constructed additional contours for all the sources by fixing the power-law slope at the best-fitting value for each source. These contours are shown with dashed lines in Fig. 2 (b) and Fig. 3 (b). For the group 1 sources, the differences between the two sets of contours were negligible so they are not shown for the sake of clarity.

We emphasize that the size of the 99% contours is not simply a function of signal-to-noise of the data. To illustrate this point, we have included a group 1 contour (NGC 5548, first observation) in the group 2 plots. We can compare this with F 9, that has the largest contours of all eleven sources. Now, the total number of photons in the 5–7 keV band in the NGC 5548 and F 9 spectra is 1240 and 1146 respectively. Thus, the significant differences in the sizes of the contours for the two sources are due to intrinsic differences in the emission-line profile, not just signal-to-noise. Furthermore, since NGC 5548 and F 9 have the lowest signal-to-noise spectra of the eleven sources, we can conclude that the relative differences in the contours in general may be due to intrinsic differences in the line shape.

Physically, what this means is that the group 1 sources have Fe K line emission, that at the *very peak* is dominated by a low-velocity emission component that is near the rest-energy of Fe I K α . This does not, of course, mean that group 1 sources do not necessarily have broad Fe K α line components. Indeed, MCG -6-30-15 is in group 1, but it has the strongest and broadest Fe K α line yet observed in an AGN. It simply means that our single-Gaussian fits are picking up a narrow component at ~ 6.4 keV that stands prominently above the underlying broad line because the latter is spread out over such a large energy range. In the group 2 sources, the *peak* line emission at ~ 6.4 keV is not dominated by a narrow component, but has a significant contribution from an underlying broad component. This could be because the narrow component is

weaker relative to the broad component than it is in group 1, *or* it could mean that the broad component is narrower than it is in group 1.

We obtained a weighted mean line center energy of 6.399 ± 0.003 keV for the seventeen out of eighteen spectra in which the line energy could be measured (see Table 1). Omitting NGC 3783(2) to avoid bias due to the very deep, ~ 850 ks exposure of this AGN, we obtained 6.404 ± 0.005 keV. Here, for the calculation of the weighted mean of any quantity with asymmetric errors, we simply assume symmetric errors, using the largest 68% confidence error in Table 1. The weighted mean FWHM of the Fe K α line cores for the fourteen data sets for which it could be measured, is 1850 ± 360 km s $^{-1}$. Without NGC 3783(2) it is 2380 ± 760 km s $^{-1}$. For the eight group 1 observations of six AGN (see Fig. 2 (a) and Fig. 3 (a)), the weighted mean line center energy and FWHM is 6.398 ± 0.003 keV and 1756 ± 366 km s $^{-1}$ respectively. For the five observations of the five sources in group 2 (see Fig. 2 (b) and Fig. 3 (b)), the weighted mean line center energy and FWHM is 6.406 ± 0.023 and 5831 ± 4046 km s $^{-1}$ respectively. At 99% confidence, the *Chandra* HEG resolves the narrow component of the Fe K α emission in three group 1 spectra (NGC 3516(2), NGC 3783(2), and NGC 5548(1)), and three group 2 spectra (Mkn 279, NGC 4051, and F 9). Interestingly, in NGC 3516 and NGC 5548 (which have multiple observations), the line is resolved in the *lower* signal-to-noise spectrum in each case. In each source the continuum level appears to be similar for the pair of observations. Therefore there appears to be real variability in the line width on a timescale of months to years, which indicates a change in the dominant distance of the line emission relative to the putative central black hole. Alternatively, it may be that there is a variable broad accretion-disk component affecting the measured width of the line core.

Fig. 2 (a) shows that for NGC 3516, NGC 3783, and NGC 5548 the 99% contours of line intensity versus center energy are less than ~ 80 eV wide and are fairly symmetrical about 6.400 keV. Thus, in these AGN, the narrow Fe K α component detected by the *HETGS* is predominantly from distant matter. The FWHM contours in Fig. 3 suggest an origin at the location of the optical BLR and/or beyond (see also Yaqoob *et al.* 2001; Kaspi *et al.* 2002; Page *et al.* 2003). Due to the symmetry of the contours around 6.400 keV,

the 99% confidence bounds imply that most of the Fe must be less ionized than Fe XV or so, with Fe I being the most likely ionization state. For 3C 120 and Mkn 509, the 99% intensity versus energy contours are ~ 70 and ~ 90 eV wide, respectively, and both contours are centered significantly above 6.400 keV (by ~ 25 eV). For these two sources, the most dominant ionization stage is likely to be Fe XVII or so, but the 99% contours do not rule out anything in the range Fe I to Fe XIX. We note that 3C 120 and Mkn 509 are two of the most luminous sources in the sample (see Table 1) so a higher ionization state for the line-emitting matter may be commensurate with this (e.g. see Nandra *et al.* 1997b). Thus, not only is the origin of the entire Fe K α line emission in these two sources controversial (3C 120: see Zdziarski & Grandi 2001; Mkn 509: see Pounds *et al.* 2001; Page, Davis, & Salvi 2003; De Rosa *et al.* 2003), the origin of the peak emission is also ambiguous.

The last source, MCG-6-30-15, has the widest intensity versus energy contour (~ 170 eV) in group 1, so the narrow Fe K α line component in this case clearly is being affected by the underlying broad line. Since the contour is symmetric about 6.4 keV, the ionization state is likely to be low (but the 99% upper limit allow ionization states up to Fe XVII). We note that the EW of the narrow-line component is about the same as that obtained by Wilms *et al.* (2001) and Ballantyne, Ross, & Fabian (2001) who included it in a complex broad plus narrow-line model applied to *XMM-Newton* data.

Strictly speaking, in all six of the group 1 sources, we cannot rule out higher ionization states than mentioned, due to the possibility of gravitational redshifts affecting the line peak. However, it seems unlikely that the dominant ionization stage of Fe and the gravitational redshifting would conspire to give a center energy so close to 6.4 keV in four of the six group 1 sources.

Of the five group 2 AGN, the Fe K α line cores in three of them are resolved (Mkn 279, NGC 4051, and F 9). This, along with the fact that the 99% contours in both center energy and line width (Fig. 2 (b) and Fig. 3 (b) respectively) are very wide, implies that the line cores in these sources are clearly dominated by a broad line. However, the fact that the line center best-fitting values are still close to 6.4 keV, and the presence of asymmetry in the contours (compared to

group 1), means that there is still an important contribution from matter that is in the outer accretion disk or far from it. In NGC 4593 and IC 4329a the line *peak* is not resolved and is stronger than in the other three group 2 sources, but not as dominant over the broad Fe K α emission as it is for the group 1 sources.

Fig. 4 shows the ratios of the spectral data to the simple fitted continuum, in the 3–8 keV band for the group 2 sources. Note that MCG –6-30-15 is a group 1 source but still has a strong broad Fe K line component. However, it is not shown in Fig. 4 since a similar plot has already been shown by Lee *et al.* (2002) and discussed at length. The data in Fig. 4 have been binned at 0.04 Å so the broad structure of the Fe K line emission in these sources is more readily apparent than in Fig. 1. However, we find that, except for IC 4329a, the signal-to-noise and bandpass of the data are insufficient to provide useful constraints on physical models from spectral fitting. In any case, this is beyond the scope of the present paper, in which we are concerned with measurements of the line cores. IC 4329a is by far the brightest AGN in the sample and detailed modeling of the complex Fe K line emission apparent in Fig. 4 is presented in McKernan, Yaqoob, & Padmanabhan (2004, in preparation). Here we simply note that one interpretation of the data for IC 4329a is that the higher-energy peak in the Fe K complex is due to Fe XXVI Ly α emission. NGC 7314 is the only other source in this *Chandra* sample with a statistically significant peak near the energy expected for Fe XXVI Ly α (see Yaqoob *et al.* 2003a). *XMM-Newton* data for MCG –6-30-15 show structure in the line emission above 6.4 keV that could either be interpreted as Fe He-like resonance absorption at ~ 6.7 keV, or Fe H-like emission at ~ 6.9 keV (Fabian *et al.* 2002). The HEG data are rather ambiguous. He-like absorption may be present but the signal-to-noise is too poor (see also Lee *et al.* 2002). In our HEG sample, there is marginal evidence for a peak near ~ 6.9 keV in 3C 120, NGC 4593, F 9, and Mkn 766. Aside from NGC 7314, emission from He-like Fe is not evident from any of the other spectra. It is also difficult to rule out He-like resonance absorption in cases where there is an underlying broad Fe K emission line, because one does not know how much broad line emission there is at the resonance energy if some of it has been absorbed.

If the core of the Fe K α line originates in an accretion disk we can obtain some simple constraints on the inclination angle and outer radius of emission given that the two Doppler peaks from the outer radius of emission are both contained within the FWHM as measured with our Gaussian fits. Note that the line profile integrated between two radii may not actually have discernable Doppler peaks, but the difference in the energies of the red and blue Doppler horns at the outer radius still sets a firm lower limit on the overall line width, assuming azimuthal symmetry of the line emission. Using a simple Schwarzschild geometry and the approximations in Yaqoob *et al.* (2003a), the condition that the line centroid is shifted by less than $\epsilon \equiv \Delta E/E_0$ is $(r/r_g) > 2[1 - (1 - \epsilon)^2]^{-1}$, where $r_g \equiv GM/c^2$. For $\Delta E = 50$ eV and $E_0 = 6.4$ keV, $r > 129r_g$. For the worst case, in which the He-like Fe K line is shifted down to 6.4 keV ($\Delta E = 280$ eV, $E_0 = 6.7$ keV), $r > 24r_g$. Now, for a given outer radius, if the disk inclination is too large, the line will be too broad. The separation of the Doppler peaks from the emission at the outer radius must be less than the FWHM, so $2\sqrt{r_g/r} \sin \theta < \text{FWHM}/c$ (e.g. see Yaqoob *et al.* 2003a). Combining this with the energy shift condition gives $\sin \theta < (\text{FWHM}/c)(2[1 - (1 - \epsilon)^2])^{-\frac{1}{2}}$. Thus for the group 1 cases in which the lines are unresolved, using $\text{FWHM} = 1860 \text{ km s}^{-1}$ and $\Delta E = 10$ eV gives a very tight constraint of $\theta < 4.5^\circ$. For $\text{FWHM} = 10,000 \text{ km s}^{-1}$ (more appropriate for 3C 120 and Mkn 509), and ΔE in the range 25 eV to 280 eV, the upper limit on θ is in the range 15.5° to 4.6° respectively. The constraints on the group 2 sources are obviously much looser. In general, if there is a significant disk contribution to the Fe K α line core, aside from the small inclination angle, there must be significant line emissivity at large radii. This would be more easily achieved if the X-ray continuum source illuminating the disk were extended over the disk (for example, the corona) rather than localized at the center of the system. Whether the continuum source is centrally localized or extended, a geometry in which the disk becomes flared at large radii would also help.

Table 1 and Fig. 3 show that the EWs of the Fe K α line core are typically in the range $\sim 40 - 200$ eV. An EW of 40 eV can easily be produced by a column density of 10^{23} cm^{-2} , covering 35% of the sky as seen from the X-ray continuum source, values that are reasonable for

the optical BLR in NGC 5548 (see discussion in Yaqoob *et al.* 2001). A line core EW of 40 eV could also conceivably be produced by the outer regions of an accretion disk view at small inclination angles (e.g. see George & Fabian 1991). However, values of EW at the higher end of the measured range ($\sim 100 - 200$ eV) require super-solar iron abundances or anisotropic illumination of the line-emitting matter by the X-ray continuum. Line-emission from a parsec-scale torus structure, that has been invoked in AGN unification schemes, could also help in accounting for the larger EWs since it could subtend a substantial solid angle at the continuum source and easily contribute another ~ 50 eV to the core EW. If the torus is optically thick a Compton-reflection continuum is predicted, commensurate with the EW of the line emission. In principle this would be a useful observational diagnostic. However, uncertainties in the Compton-thickness of the torus, the iron abundance, the contribution to the reflection continuum from the outer disk, and the amount of line contribution from the (optically-thin) BLR, not to mention the measurement uncertainties in the reflection continuum itself, make it difficult to draw robust conclusions from correlating the line EW with the strength of the reflection continuum. The situation is sufficiently complicated that these tests must be done on a source-by-source basis and is beyond the scope of the present paper. We note also that the precision of our new measurements of peak energy, core FWHM, and EW will allow more stringent tests of alternative models of the origin of the Fe K α line emission than has hitherto been possible (e.g. see Sulentic *et al.* 1998; Elvis 2000).

The authors thank Ian George, Jane Turner, Barry McKernan, James Reeves, Richard Mushotzky, Sergei Nayakshin, Kim Weaver, and Peter Serlemitsos for valuable discussions, and an anonymous referee for helping to improve the paper. Support for this work was provided by NASA through *Chandra* Award Numbers GO2-2102X, and GO2-3133X issued by the Chandra X-ray Observatory Center, which is operated by the Smithsonian Astrophysical Observatory for and on behalf of the NASA under contract NAS8-39073. The authors also gratefully acknowledge support from NASA grants NCC5-447 (T.Y., U.P.), and NAG5-10769 (T.Y.). This research made use of the HEASARC online data archive services, sup-

ported by NASA/GSFC. This research has made use of the NASA/IPAC Extragalactic Database (NED) which is operated by the Jet Propulsion Laboratory, California Institute of Technology, under contract with NASA. The authors are grateful to the *Chandra* instrument and operations teams for making these observations possible.

REFERENCES

1. Arnaud, K. A. 1996, *Astronomical Data Analysis Software and Systems V*, eds. Jacoby, G., & Barnes, J., p. 17, ASP Conference Series, Vol. 101
2. Ballantyne, D., Ross, R. R., & Fabian, A. C. 2001, *MNRAS*, 327, 10
3. Collinge, M. J., *et al.* 2001, *ApJ*, 557, 2
4. De Rosa, A., Piro, L., Matt, G., & Perola, G. C. 2003, *A&A*, in press (astro-ph/0309699)
5. Done, C., Madejski, G. M., & Życki, P. T. 2000, *ApJ*, 536, 213
6. Elvis, M. 2000, *ApJ*, 545, 63
7. Fabian, A. C., Iwasawa, K.; Reynolds, C. S., & Young, A. J. 2000, *PASP*, 112, 1145
8. Fabian, A. C., *et al.* 2002, *MN*, 335, L1
9. Gehrels, N. 1986, *ApJ*, 303, 336
10. George, I. M., & Fabian, A. C. 1991, *MN*, 249, 352
11. Gondoin, P., Orr, A., Lumb, D., & Siddiqui, H. 2003, *A&A*, 397, 883
12. Kaastra, J. S., *et al.* 2002, in ASP Conf. Ser. 290, *Active Galactic Nuclei: From Central Engine to Host Galaxy*, ed. S Collin, F. Combes, & I. Shlosman, (San Francisco: ASP), 101
13. Kaspi, S., *et al.* 2001, *ApJ*, 554, 216
14. Kaspi, S., *et al.* 2002, *ApJ*, 574, 643
15. Lee, J. C., Iwasawa, K., Houck, J. C., Fabian, A. C., Marshall, H. L., & Canizares, C. R. 2002, *ApJ*, 570, L47
16. Lubiński, P., & Zdziarski, A. A. 2001, *MNRAS*, 323, L37
17. Markert, T. H., Canizares, C. R., Dewey, D., McGuirk, M., Pak, C., & Shattenburg, M. L. 1995, *Proc. SPIE*, 2280, 168
18. Nandra, K., George, I. M., Mushotzky, R. F., Turner, T. J., & Yaqoob, T. 1997a, *ApJ*, 477, 602
19. Nandra, K., George, I. M., Mushotzky, R. F., Turner, T. J., & Yaqoob, T. 1997b, *ApJ*, 488, L91
20. Netzer, H., *et al.* 2003, *ApJ*, in press (astro-ph/0309096)
21. Page, K. L., O'Brien, P. T., Reeves, J. N., & Turner, M. J. L. 2003, *MN*, in press (astro-ph/0309394)
22. Page, M. J., Davis, S. W., & Salvi, N. J. 2003, *MN*, 343, 1241
23. Perola, G. C., Matt, G., Cappi, M., Fiore, F., Guainazzi, M., Maraschi, L., Petrucci, P. O., & Piro, L. 2002, *A&A*, 389, 802
24. Petrucci, P. O., *et al.* 2002, *A&A*, 388, L5
25. Pounds, K. A., Reeves, J. N., Page, K. L., Wynn, G. A., & O'Brien, P. T. 2003, *MN*, 342, 1147
26. Reeves, J. N. 2002, in ASP Conf. Ser., *Active Galactic Nuclei, from Central Engine to Host Galaxy*, ed. S Collin, F. Combes & I. Shlosman, (San Francisco: ASP), 35
27. Reeves, J. N., Nandra, K., George, I. M., Pounds, K. A., Turner, T. J., Yaqoob, T. 2004, *ApJ*, in press (astro-ph/0310820)
28. Reynolds, C. S., & Nowak, M. A. 2003, *Phys. Rep.*, 377, 389
29. Sulentic, J. W., Marziani, P., Zwitter, T., Calvani, M., & Dultzin-Hacyan, D. 1998, *ApJ*, 501, 54
30. Turner, T. J., *et al.* 2002, *ApJ*, 574, L123
31. Turner, T. J., Romano, P., George, I. M., Edelson, R., Collier, S. J., Mathur, S., & Peterson, B. M. 2001, *ApJ*, 561, 131
32. Vignali, C., Brandt, W. N., Boller, Th., Fabian, A. C., Vaughan, S. 2004, in press (astro-ph/0310278)
33. Weaver, K. A., Gelbord, J., & Yaqoob, T. 2001, *ApJ*, 550, 261
34. Wilms, J., Reynolds, C. S., Begelman, M. C., Reeves, J., Molendi, S., Staubert, R., & Kendziorra, E. 2001, *MN*, 328, L27
35. Yaqoob, T., George, I. M., Nandra, K., Turner, T. J., Serlemitsos, P. J., & Mushotzky, R. F. 2001, *ApJ*, 546, 759
36. Yaqoob, T., George, I. M., Kallman, T. R., Padmanabhan, U., Weaver, K. A., & Turner, T. J. 2003a, *ApJ*, 596, 85
37. Yaqoob, T., McKernan, B., Kraemer, S. B., Crenshaw, D. M., Gabel, J. R., George, I. M., & Turner, T. J. 2003b, *ApJ*, 582, 105
38. Yaqoob, T., Padmanabhan, U., Dotani, T., & Nandra, K. 2002, *ApJ*, 589, 487
39. Zdziarski, A. A., & Grandi, P. 2001, *ApJ*, 551, 186

Table 1

Chandra Parameters of the Core Fe K Line Emission from *Chandra* (HEG) Data

Source, & Refs. ^g	z^a	E^b (keV)	I^c	EW ^d (eV)	FWHM ^e (km s ⁻¹)	F^f L^f
NGC 7314	0.004760	$6.412^{+0.010}_{-0.015}$	$1.7^{+0.6}_{-0.8}$	48^{+17}_{-23}	100 f	3.0
[1]		(6.395 – 6.430)	(0.7 – 2.7)	(20 – 76)	...	0.15
NGC 3516(1)	0.008836	$6.398^{+0.017}_{-0.007}$	$4.0^{+1.3}_{-1.2}$	140^{+46}_{-42}	1290^{+1620}_{-1290}	2.3
[2]		(6.389 – 6.408)	(2.5 – 5.8)	(88 – 203)	(0 – 3630)	0.40
NGC 3516(2)	0.008836	$6.401^{+0.015}_{-0.017}$	$3.8^{+1.5}_{-1.3}$	143^{+56}_{-49}	3630^{+2350}_{-1540}	2.1
[2]		(6.378 – 6.422)	(2.2 – 5.8)	(83 – 218)	(1560 – 7640)	0.35
Mkn 509	0.034397	$6.430^{+0.024}_{-0.023}$	$3.1^{+1.9}_{-1.6}$	54^{+33}_{-28}	2820^{+2680}_{-2800}	5.3
...		(6.394 – 6.461)	(0.9 – 5.7)	(16 – 99)	(0 – 7710)	14.0
NGC 5548(1)	0.016760	$6.397^{+0.019}_{-0.023}$	$3.1^{+1.5}_{-1.2}$	115^{+56}_{-45}	3750^{+2590}_{-1890}	2.4
[3]		(6.365 – 6.422)	(1.5 – 5.1)	(56 – 189)	(1250 – 7610)	1.5
NGC 5548(2)	0.016760	$6.400^{+0.010}_{-0.010}$	$2.1^{+0.8}_{-0.7}$	67^{+26}_{-22}	1780^{+1420}_{-1220}	2.9
[4]		(6.386 – 6.414)	(1.2 – 3.3)	(38 – 105)	(0 – 3970)	1.8
3C 120	0.033010	$6.415^{+0.017}_{-0.017}$	$3.0^{+1.8}_{-1.5}$	61^{+37}_{-31}	2000^{+2950}_{-2000}	4.4
...		(6.392 – 6.450)	(1.1 – 5.5)	(22 – 112)	(0 – 6770)	10.8
NGC 4593	0.008301	$6.403^{+0.012}_{-0.038}$	$3.4^{+3.2}_{-1.3}$	80^{+75}_{-31}	2140^{+8370}_{-1230}	4.1
...		(6.349 – 6.434)	(1.8 – 8.1)	(42 – 191)	(310 – 15920)	0.63
NGC 3783(1)	0.009730	$6.400^{+0.014}_{-0.016}$	$5.0^{+2.4}_{-2.1}$	73^{+35}_{-31}	2550^{+2420}_{-1560}	6.0
[5]		(6.376 – 6.420)	(2.4 – 8.3)	(35 – 121)	(500 – 6290)	1.2
NGC 3783(2)	0.009730	$6.397^{+0.003}_{-0.003}$	$4.9^{+0.6}_{-0.5}$	70^{+9}_{-7}	1700^{+410}_{-390}	6.2
[6, 7]		(6.393 – 6.401)	(4.2 – 5.6)	(60 – 80)	(1180 – 2250)	1.3
MCG -6-30-15	0.007749	$6.408^{+0.030}_{-0.025}$	$1.6^{+1.1}_{-0.9}$	49^{+34}_{-28}	3250^{+5230}_{-3250}	3.2
[8]		(6.349 – 6.454)	(0.4 – 3.3)	(12 – 101)	(0 – 12670)	0.42
Mkn 279	0.030451	$6.415^{+0.047}_{-0.027}$	$1.9^{+1.0}_{-0.9}$	132^{+69}_{-63}	5010^{+6550}_{-2810}	1.3
...		(6.379 – 6.521)	(0.7 – 5.2)	(49 – 361)	(1100 – 36980)	2.7
NGC 4051	0.002336	$6.419^{+0.038}_{-0.033}$	$3.2^{+1.7}_{-1.4}$	191^{+101}_{-84}	6330^{+7740}_{-3330}	1.6
[9]		(5.910 – 6.475)	(1.4 – 25.0)	(84 – 1492)	(1780 – 137470)	0.019
IC 4329A	0.016094	$6.309^{+0.089}_{-0.099}$	$11.3^{+7.2}_{-6.4}$	62^{+40}_{-35}	15090^{+12430}_{-9950}	16.4
...		(6.171 – 6.468)	(1.8 – 21.3)	(10 – 117)	(0 – 37150)	9.4
F 9	0.047016	$6.373^{+0.254}_{-0.092}$	$4.9^{+8.7}_{-3.3}$	216^{+384}_{-145}	17040^{+55960}_{-14270}	2.1
...		(6.203 – 6.753)	(1.2 – 17.0)	(53 – 749)	(2160 – 92940)	10.6
Mkn 766	0.012929	$6.423^{+0.018}_{-0.016}$	$0.7^{+0.6}_{-0.5}$	34^{+29}_{-24}	100 f	2.1
...		(6.398 – 6.456)	(0.1 – 1.5)	(5 – 73)	...	0.79
NGC 3227	0.003859	$6.384^{+0.015}_{-0.016}$	$1.1^{+1.2}_{-0.9}$	39^{+43}_{-32}	100 f	2.3
...		...	(0 – 2.8)	(0 – 99)	...	0.075
Akn 564	0.024684	6.400 f	$0.3^{+0.5}_{-0.3}$	16^{+27}_{-16}	100f	2.5
[10]		...	(0.0 – 1.1)	(0 – 59)	...	3.4

Chandra HEG data, fitted with a power law plus Gaussian emission line model in the 2–7 keV band (for NGC 3516 photoelectric absorption was also included in the model). All parameters (except redshift) were free in the fits, except in the cases of NGC 7314, Mkn 766, NGC 3227 (line width fixed in these cases), and Akn 564 (line energy and width fixed). All parameters are quoted in the source rest frame. Statistical errors are for the 68% confidence level, whilst parentheses show the 90% confidence level ranges of the parameters. The number of interesting parameters assumed for calculating the statistical errors was equal to the number of free parameters in the Gaussian component of the model. For 3, 2, and 1 interesting parameter(s), the corresponding values of ΔC for 68% confidence are 3.506, 2.279 and 0.989 respectively. For 3, 2, and 1 interesting parameter(s), the 90% confidence values of ΔC are 6.251, 4.605 and 2.706 respectively. ^a Redshifts obtained from NASA Extragalactic Database (NED). ^b Gaussian line center energy. ^c Emission-line intensity in units of 10^{-5} photons cm⁻² s⁻¹. ^d Emission line equivalent width. ^e Full width half maximum, rounded to 10 km s⁻¹. ^f F is the estimated 2–10 keV observed flux in units of 10^{-11} ergs cm⁻² s⁻¹. The power-law continuum was extrapolated to 10 keV. L is the estimated 2–10 keV source-frame luminosity (using the 2–10 keV estimated flux), in units of 10^{43} ergs s⁻¹, assuming $H_0 = 70$ km s⁻¹ Mpc⁻¹ and q_0 . ^g Key for previous publications on the same HEG data: [1] Yaqoob *et al.* 2003a, [2] Turner *et al.* 2002, [3] Yaqoob *et al.* 2001, [4] Kaastra *et al.* 2002, [5] Kaspi *et al.* 2001, [6] Kaspi *et al.* 2002, [7] Netzer *et al.* 2003, [8] Lee *et al.* 2002, [9] Collinge *et al.* 2001, [10] Mastumoto, Leighly, & Marshall 2001, http://www.pha.jhu.edu/groups/astro/workshop2001/papers/matsumoto_c.ps.

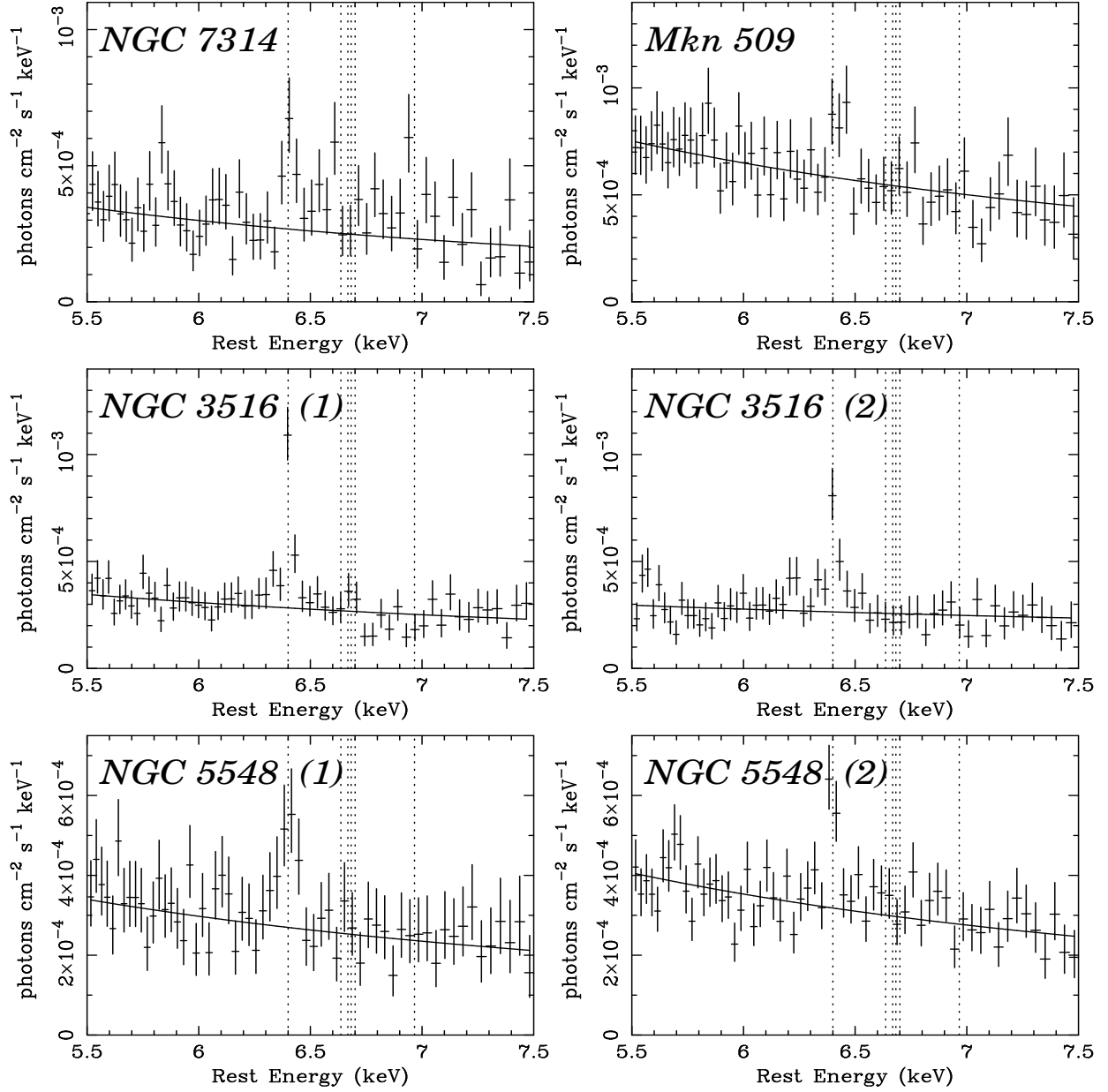
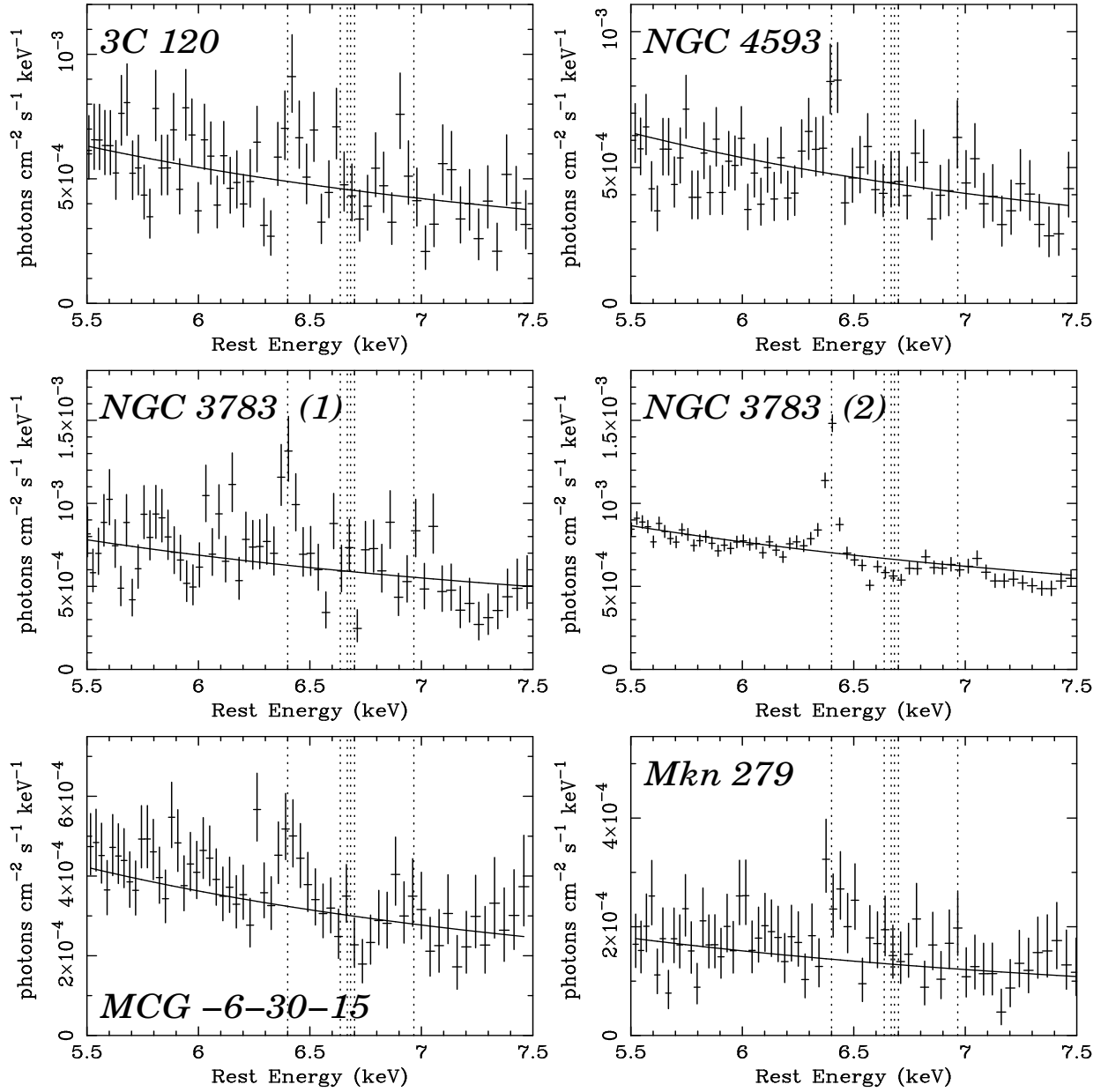
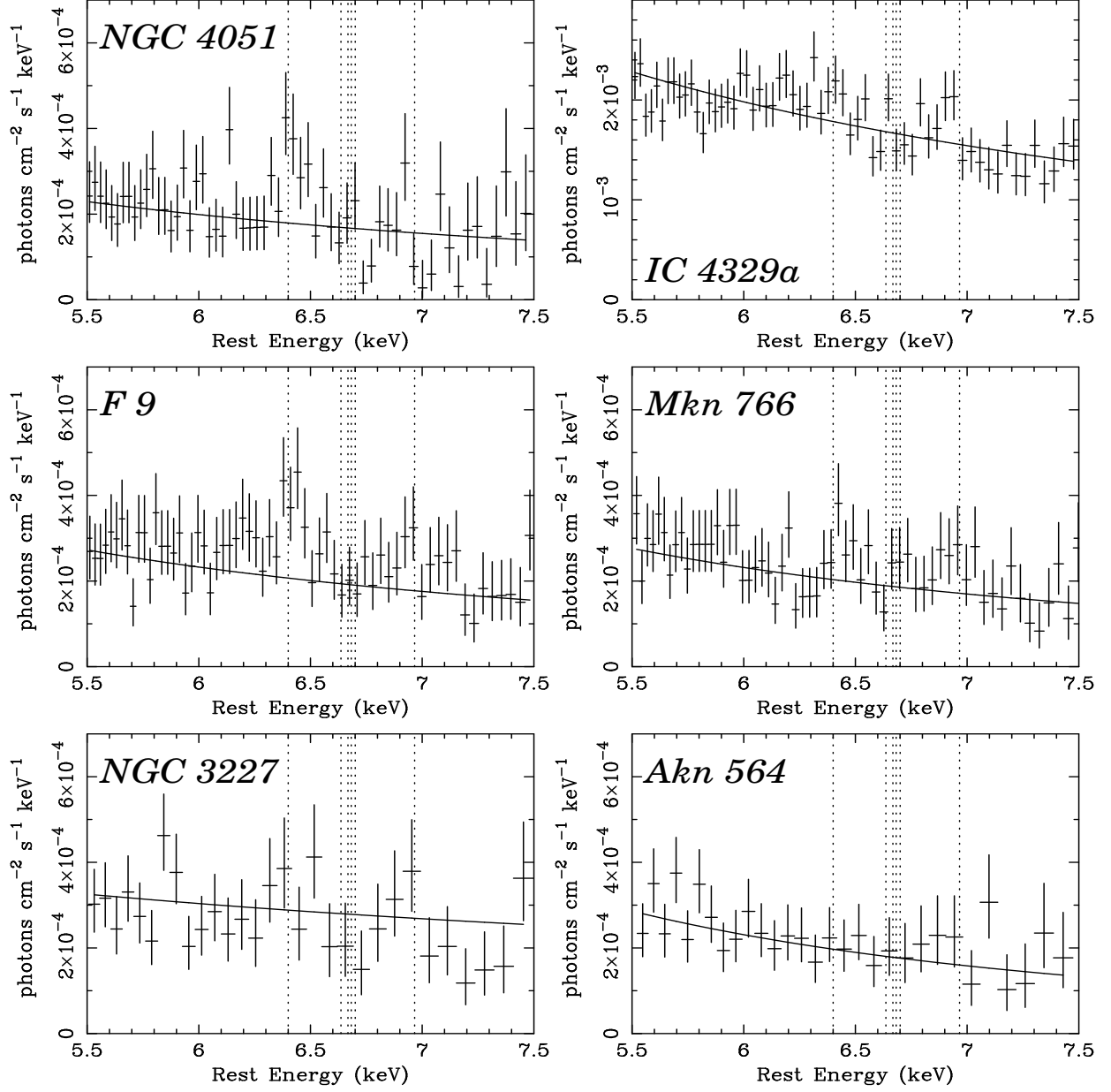


Figure 1. *Chandra* HEG spectra in the Fe K band from each of the eighteen observations of fifteen type I AGN (see Table 1). The data are binned at 0.01\AA for the first sixteen spectra shown, and 0.02\AA for the last two spectra (NGC 3227 & Akn 564). This can be compared to the HEG spectral resolution, which is 0.012\AA FWHM. The data are combined from the -1 and $+1$ orders of the grating. The spectra have been corrected for instrumental effective area and cosmological redshift. Note that these are *not* unfolded spectra and are therefore independent of the model that is fitted. The statistical errors shown correspond to the 1σ Poisson errors, calculated using equations (7) and (14) in Geherls (1986) to approximate the upper and lower errors respectively. The solid line corresponds to the continuum model fitted over the $2\text{--}7$ keV range (extrapolated to 7.5 keV), as described in the text (§3). The vertical dotted lines represent (from left to right), the rest energies of the following transitions: Fe I $K\alpha$, Fe XXV forbidden, two intercombination lines of Fe XXV, Fe XXV resonance, and Fe XXVI $\text{Ly}\alpha$. The spectrum for NGC 7314 corresponds to that during a low continuum state, as defined and described in Yaqoob *et al.* 2003a. Note that an apparent narrow feature at ~ 6.35 keV in MCG $-6\text{--}30\text{--}15$ and at ~ 6.55 keV in NGC 3783(2) are detected in one arm of the grating only and are narrower than the spectral resolution, so are not real.

Figure 1. – *continued*

Figure 1. – *continued*

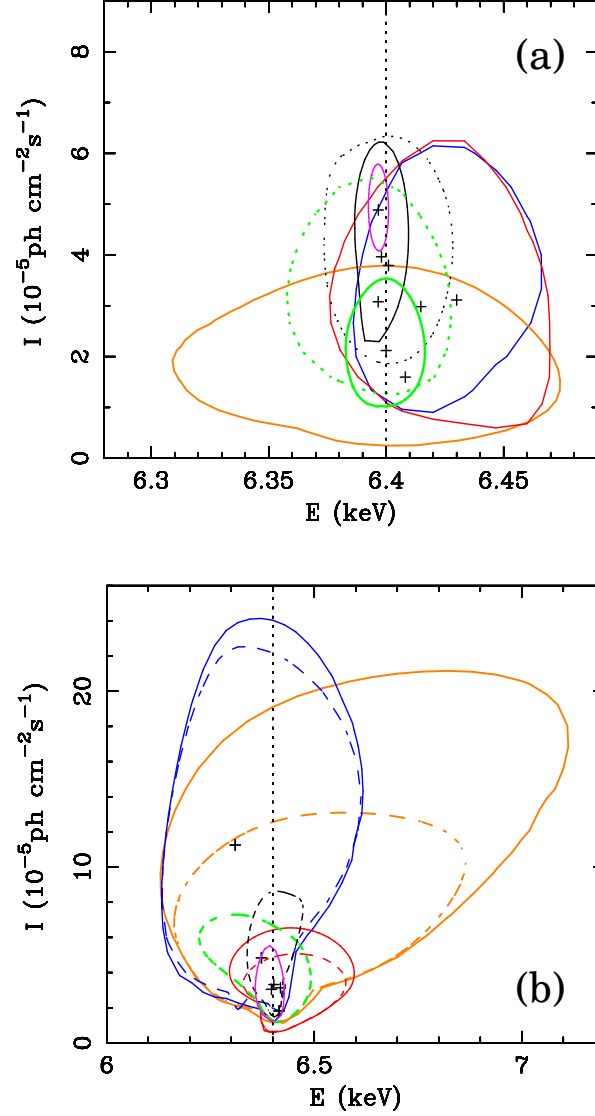


Figure 2. (a) Joint 99% confidence contours of the Fe K α emission-line core intensity versus line center energy obtained from Gaussian fits to the line as described in the text, for eight observations of six AGN: NGC 3516 (black), Mkn 509 (red), NGC 5548 (green), 3C 120 (blue), NGC 3783 (magenta), and MCG-6-30-15 (brown). See also Table 1 and Fig. 3. Dotted contours are for the same source but from a different observation (the dotted contours are for the lowest signal-to-noise spectrum of the pair in each case). Note that the very smallest contour (magenta) is from the ~ 850 ks observation of NGC 3783. The first observation of NGC 3783 was excluded from the plot because it is has a factor of ~ 20 less exposure time. Also excluded were NGC 7314 (Fe K line emission was very complex), and Mkn 766, NGC 3227, and Akn 564, that all had insufficient signal-to-noise to obtain well-constrained contours. (b) As (a), for five more AGN: NGC 4593 (black), Mkn 279 (red), NGC 4051 (green), IC 4329a (blue), and F 9 (brown). Also shown here is the 99% contour for NGC 5548(1) (magenta, and the smallest contour in the plot) to compare with the contour of F 9. These two data sets have a similar number of counts in the 5–7 keV spectra but the size and shape of the contours are completely different. This shows that the differences in the size and shape of the contours in general reflect intrinsic differences in the line profile shapes. The dashed contours were obtained by fixing the power-law continuum slope after finding the best fit because closed contours could not be obtained otherwise for NGC 4593 (black) and NGC 4051 (green). For the sources in Fig. 2 (a), the contours obtained by freezing the continuum slopes at the best-fitting values were not significantly different from the fits with all parameters free, so they are not shown for clarity.

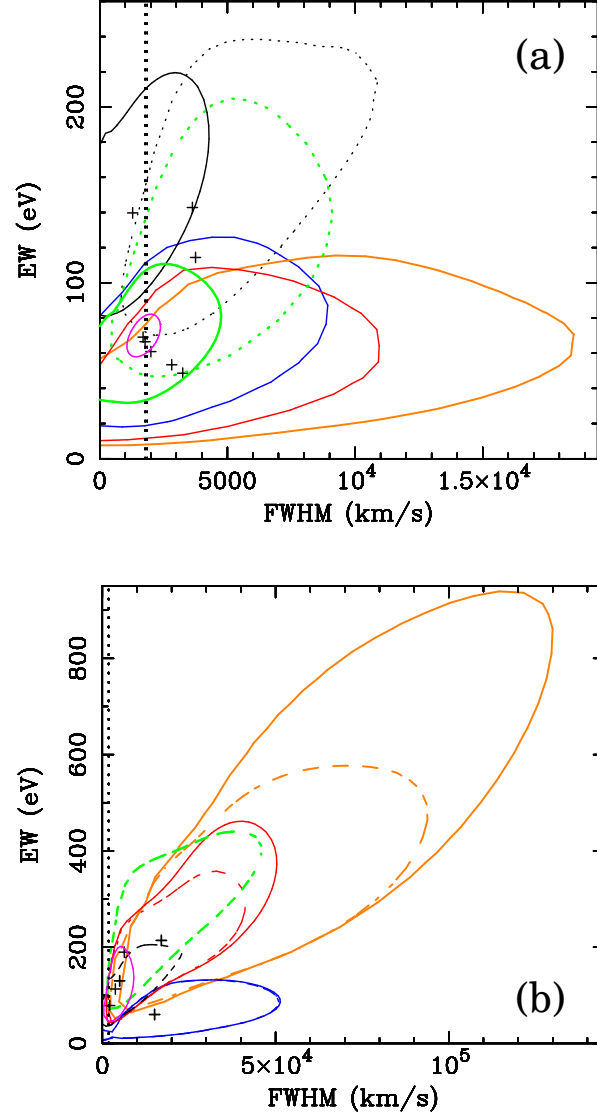


Figure 3. (a) Joint 99% confidence contours of the Fe K α emission-line core equivalent width (EW) versus velocity width FWHM, for the same six AGN as in Fig. 2 (a), using the same color coding. (b) As (a) but for the same five AGN as in Fig. 2 (b), using the same color coding. Note that the FWHM was calculated simply from $v/c = 2.35\sigma/E_0$, where E_0 is the line center energy and σ is the Gaussian line width. Strictly speaking, this is valid only for $v/c \ll 1$ so the conversion is not accurate for the highest velocity parts of the contours. Again NGC 5548(1) from Fig. 3 (a) is included for comparison (small, magenta contour). The dashed contours were obtained by freezing the power-law continuum slope at the best-fitting value: for NGC 4593 (black) and NGC 4051 (green) closed contours could only be obtained in this way. See also caption to Fig. 2 (b).

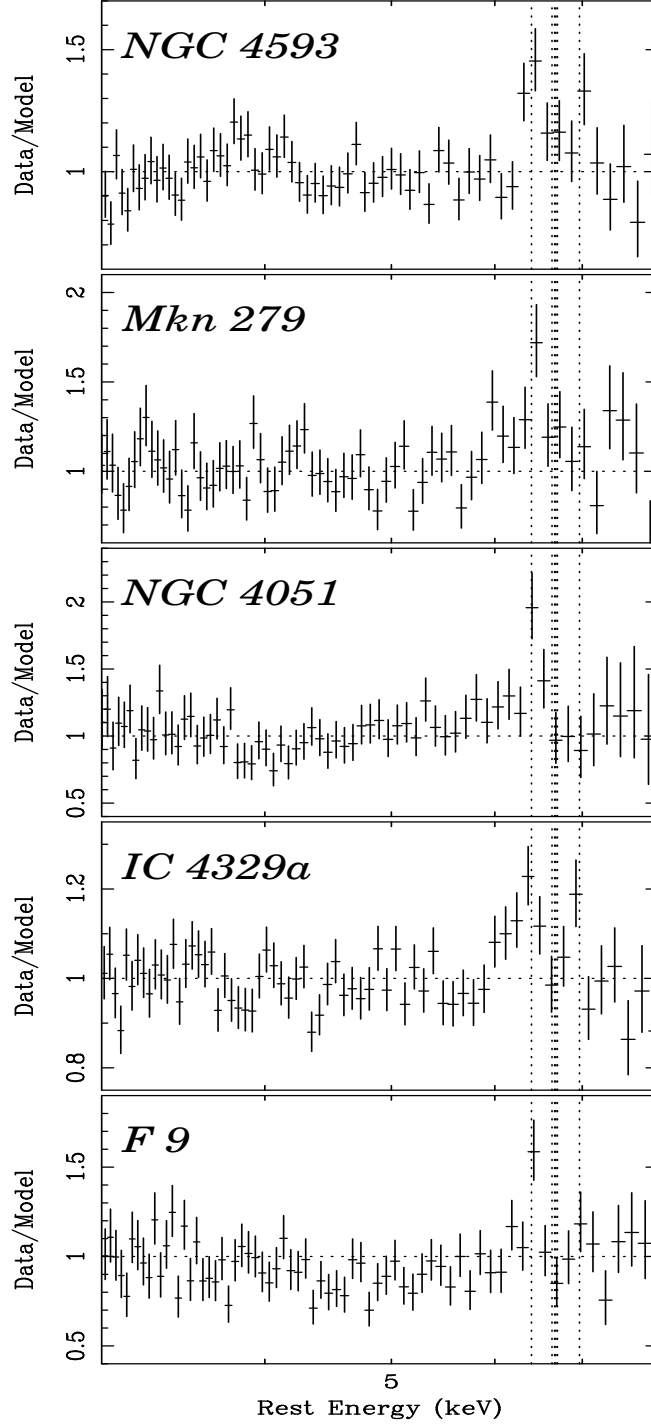


Figure 4. Ratios of HEG data to a simple power-law continuum model (fitted as described in the text, §3) for five AGN in Fig. 1 and Table 1 which show evidence of broad and/or complex Fe K line emission. MCG -6-30-15 is not shown, since a similar plot has already been shown in Lee *et al.* (2002). The data are binned at 0.04\AA , coarser than the HEG spectral resolution (0.012\AA FWHM). The data are combined from the -1 and $+1$ orders of the grating. The spectra have been corrected for instrumental effective area and cosmological redshift. The statistical errors shown correspond to the 1σ Poisson errors, calculated using equations (7) and (14) in Geherls (1986) to approximate the upper and lower errors respectively. The vertical dotted lines represent (from left to right), the rest energies of the following transitions: Fe I $K\alpha$, Fe XXV forbidden, two intercombination lines of Fe XXV, Fe XXV resonance, and Fe XXVI $Ly\alpha$.